Journal of
Materials Chemistry A

Materials for energy and sustainability

Accepted Manuscript

This article can be cited before page numbers have been issued, to do this please use: X. Yan, C. Shi, J. Wu, K. J. Chen and Z. Yang, *J. Mater. Chem. A*, 2026, DOI: 10.1039/D5TA09690A.

ROYAL SOCIETY OF CHEMISTRY

rsc.li/materials-a

View Article Online
DOI: 10.1039/D5TA09690A

A bismuth ferrite-based lead-free piezoelectric ceramic surpassing PZT-8 in thermal stability

Xiaodong Yan[1], Chaoyang Shi[2], Jianjun Wu[3], Kevin Chen[4*], Zhengbao Yang[1*]

[1]Department of Mechanical and Aerospace Engineering, The Hong Kong University of Science and Technology, Clear Water Bay, Hong Kong, China
[2]School of Mechanical Engineering, Tianjin University, Tianjin, 300072, China
[3]Sichuan Energy Investment Tianfu Clean Energy Research Institute, Chengdu, 610041, China
[4]Department of Electronic and Computer Engineering, The Hong Kong University of Science and Technology, Clear Water Bay, Hong Kong, China

Abstract

Piezoelectric materials are essential for electronics but suffer from thermal instability, especially lead-free alternatives to lead zirconate titanate (PZT). The absence of quantitative thermal stability metrics has hindered progress. In this work, we introduce a new index, denoted as "S_d", which accounts for both the operating temperature range and the central operating temperature, allowing for a comprehensive assessment. Applying this criterion, we found that the commercial PZT-4 material exhibits the highest thermal stability among the ceramics tested, confirming its reputation as the industry standard. Notably, we developed a new lead-free piezoelectric ceramic based on bismuth ferrite that achieved stable piezoelectric coefficient at 38–247 °C, the corresponding S_d value (173) exceeds that (163) of commercial PZT-8 (20–232 °C). Further analysis revealed that reducing the concentration of point defects improved its electrical homogeneity and reduced conductivity, leading to enhanced thermal stability. This work provides a new evaluation framework that can accelerate the development of thermally stable lead-free piezoelectric materials. The implications of this research extend beyond piezoelectrics, as the S_d index could find broader application in the characterization of other functional oxides.

Key words: Piezoelectric ceramic; bismuth ferrite; conductivity; defect dipole; ferroelectric.

View Article Online
DOI: 10.1039/D5TA09690A

1. Introduction

Piezoelectric materials can achieve mutual conversion between mechanical energy and electrical energy, and are key components in sensors, transducer, and actuators.[1-3] With the increasing requirement on piezoelectric devices in extreme environment, such as aerospace and deep petroleum exploration,[4] the large piezoelectricity with good temperature stability has become an urgent need. Due to its excellent performance,[5-7] PZT dominates the market for more than half a century. Unfortunately, PZT is now facing worldwide legislative restriction due to its toxicity, and this has triggered a worldwide search for Pb-free substitutes.[7-12]

Currently, the main lead-free piezoelectric materials include $BaTiO_3$ (BT)-based, (K, Na)NbO_3 (KNN)-based, $(Na_{0.5}Bi_{0.5})TiO_3$ (NBT)-based and $BiFeO_3$ (BF)-based perovskite systems. Among them, the $BiFeO_3$-based ferroelectrics, such as bismuth ferrite-barium titanate ($BiFeO_3$-$BaTiO_3$, BF-BT) possess high Curie temperature and strong spontaneous polarization,[13-17] making them potential alternatives to lead-containing piezoelectrics. However, high dielectric loss and high conductivity severely hinder stability of their piezoelectric properties.[13, 15] It was reported that the small-signal piezoelectric coefficient presents a large fluctuation (as high as 50% from 25 °C to 150 °C),[18] and the large-signal piezoelectric coefficient maintains stable below 150 °C or even lower due to the leakage.[19-21]

In addition, there is no international standard to evaluate the temperature stability of piezoelectricity. By referring to the evaluation method of the stability of capacitors,[22-24] we know that the temperature coefficient of piezoelectricity (*TCP*) can be defined usually by the formula as follow:

View Article Online
DOI: 10.1039/D5TA09690A

$$TCP = \frac{\Delta d_{33}}{d_{33,b}} = \frac{d_{33,T} - d_{33,b}}{d_{33,b}} \quad (1)$$

where the $d_{33,\ T}$ is the piezoelectric coefficient under any temperature T, the $d_{33,b}$ is the piezoelectric coefficient under the benchmark temperature. Researchers usually set room temperature as the benchmark temperature. For high temperature applications, materials need to work at 200 °C or even 300 °C, thereby, it is unreasonable to use 25 °C as the benchmark. Following the international standard on capacitance,[22, 24] the values of $TCP \leq \pm 15\%$ were considered to be the temperature-stable range, however, it is not completely applicable to the piezoelectric coefficient because of the permanent decay of piezoelectricity at the temperature where the d_{33} reaches the last peak (usually at the de-polarization temperature, T_d). Here, the low and high temperature boundaries determined by *TCP* conditions were denoted as T_l and T_h, respectively. As shown in **Fig. 1a**, for case one, the T_d is higher than the T_h, the eventual stable range is consistent with that determined by *TCP* conditions. But for case two (**Fig. 1b**), the T_d is much lower than the T_h, thereby, the upper limit temperature of the stable range is equal to T_d rather than T_h. Unfortunately, the researchers seldom discuss and even ignore this difference,[4, 25, 26] which severely limits the development of high temperature piezoelectric materials.

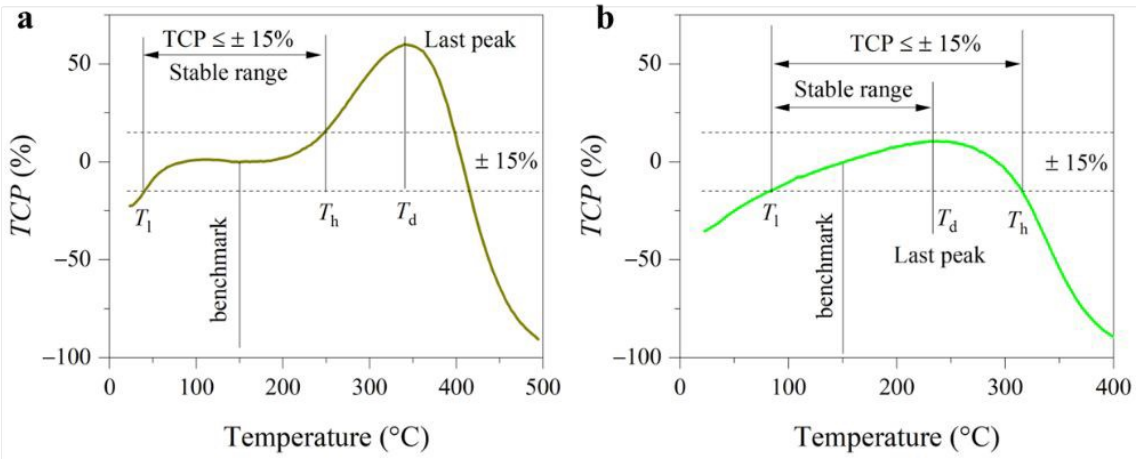

Fig. 1 Determination of the temperature-stable range. To simplify, the low and high temperature boundaries determined by *TCP* conditions are named T_l and T_h. **a**, For the case one, since the temperature where the last peak occurs (T_d) is higher than the T_h, the upper limit temperature (T_{max}) of the stable range is equal to the T_h. **b**, For the case two, the T_d is lower than the T_h, therefore, the T_{max} is equal to the T_d. As a result, the T_{max} should be taken as the smaller of the T_h and the T_d.

Here, based on the redefinition of the temperature-stable range, we propose a new criterion for evaluating the stability of piezoelectricity. Specifically, this criterion emphasizes that both high operating temperature and wide temperature range are crucial for temperature-stability (a new stability index) of piezoelectric coefficient d_{33}. We calculated the index value of different piezoceramics and find the highest value of up to 224 belongs to PZT-4, the well-known piezoceramic with the widest temperature range and high operated temperature. In contrast, within the lead-free piezoceramic category, we did not identify any materials that match the performance of their lead-based counterparts. To address this gap, we designed new lead-free ceramic (Sm doped $0.7BiFeO_3$-$0.3BaTiO_3$, composition near morphotropic phase boundary[15]) with an index value of 173 (temperature-stable range of 38–247 °C), much higher than that of undoped counterpart (152), and even comparable to that (163) of the PZT-8 (20–232 °C). We further analyzed the origins of the temperature-stable piezoelectricity in the doped $BiFeO_3$-$BaTiO_3$ ceramics. Our results indicate that a significantly reduced concentration of point defects enhances electrical homogeneity and decreases conductivity, contributing to improved thermal stability.

2. Results and discussion

View Article Online
DOI: 10.1039/D5TA09690A

2.1 The new metric of temperature stability of piezoelectricity

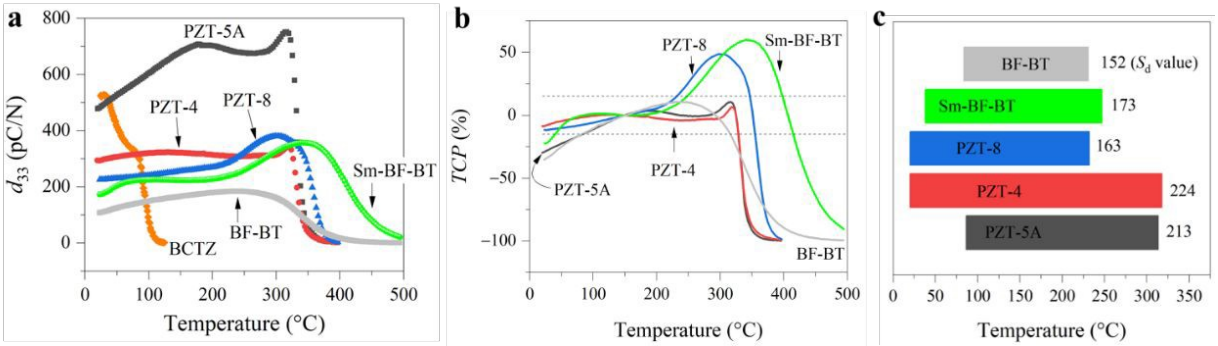

Fig. 2 The evaluation on temperature stability of piezoelectricity. **a**, The piezoelectric coefficient d_{33} of lead-free BCTZ, BF-BT, Sm-doped BF-BT and the commercial PZTs. **b**, the temperature coefficient, **c**, temperature-stable range, and thermal stability metric S_d of d_{33} of the lead-free Sm-doped BF-BT and the commercial PZTs based on the benchmark of 150 °C.

We first selected the classical materials including the commercial PZTs and lead-free ones to verify reliability. **Fig. 2a** shows the piezoelectric coefficients of the BF-BT, Sm-doped BF-BT, (Ba, Ca)(Ti, Zr)O_3 (BCTZ)[27] and the commercial PZTs under the various temperatures. For the BCTZ ceramic, d_{33} is approximately 500 pC/N at room temperature, but it is extremely sensitive to temperature due to low Curie temperature and polymorphic phase transition.[28, 29] For the PZT family, their piezoelectric coefficients have no obvious decay until to near 300 °C. Among them, PZT-5A, a soft piezoelectric material, shows a highest d_{33} value and a large fluctuation with temperature. In comparison, the hard PZTs (PZT-4 and PZT-8) show the more stable d_{33} values. Interestingly, although the d_{33} value of the Sm-BF-BT at room temperature is slightly lower than that of the hard PZT-8, it is more resistant to high temperatures. We calculate the temperature coefficient of piezoelectricity (*TCP*) according to the formula (1). In view that the high temperature piezoelectric devices need to work at 300 °C or above,[4] the benchmark

View Article Online
DOI: 10.1039/D5TA09690A

temperature was set as 150 °C. Thereby, temperature-stable range of the piezoelectric coefficient is identified preliminary based on the $TCP \leq \pm 15\%$,[22] as shown in **Fig. 2b**. Apart from the *TCP* conditions, we considered the permanent decay of piezoelectric coefficient at de-polarization temperature (T_d). For the PZT-4, PZT-5A and BF-BT, because T_d is lower than the high temperature boundary (T_h) determined by *TCP* conditions, the former is determined as the upper limit temperature (T_{max}) of the temperature-stable range. **Fig. 2c** shows the stable range of the d_{33} of lead-free BF-BT, Sm-BF-BT and PZTs. It can be found that PZT-4 has the widest temperature range (20–318 °C). PZT-8 (20–232 °C) is more stable than PZT-5A (86–314 °C) at below 200 °C, but it is inferior to the latter at higher temperature, even not as stable as the lead-free Sm-BF-BT (38–247 °C). Obviously, this comparison is still not intuitive enough.

To quantify this difference, we propose a new index to evaluate the stability of piezoelectric coefficient d_{33} (S_d) as follows:

$$S_d = \sqrt{\Delta T \cdot T_{center}} = \sqrt{(T_{max} - T_{min}) \cdot \frac{T_{max} + T_{min}}{2}} \quad (2)$$

where the T_{max} and T_{min} are the upper and the lower limit temperature in the temperature range of the stable d_{33}. The formula (2) is valid and applicable only when the temperature is above zero. A large ΔT means a wide temperature range, and high T_{center} means a high operating temperature. The importance of ΔT is obvious, T_{center} is also essential because the piezoelectric materials usually suffer from de-polarization problem when temperature arises. As the stability of piezoelectric coefficient d_{33} is closely related to temperature (including phase transition temperature and Curie temperature), we take the square root of the product of ΔT and T_{center} as S_d, which will make its unit consistent with the temperature. Although the index S_d has no

View Article Online
DOI: 10.1039/D5TA09690A

specific physical meaning, it is deduced by combining the evaluation criteria for temperature stability of capacitor and de-polarization of piezoelectric material, is more practical for judging temperature stability among various material system. The higher the S_d value is, the better the temperature stability is. For ferroelectric materials, the piezoelectric properties are only suppressed at low temperatures due to the weakened domain wall motion, while they will suffer permanent degradation at high temperatures. Therefore, the stability at high temperature (above room temperature) was paid more attention.

According to formula (2), we calculated the S_d value of the lead-free BF-BT, Sm-BF-BT and PZTs, as marked in **Fig. 2c**. The highest S_d value was obtained in PZT-4 thanks to its wide temperature range and a high upper limit temperature, which is consistent with previous cognition that PZT-4 is one of the most stable piezoelectric materials[30]. Due to a low upper-limit temperature, the S_d value of PZT-8 is much lower than PZT-4 and PZT-5A. In addition, we find that the S_d value (173) of the Sm doped BF-BT (temperature range of 38–247 °C) is higher than that (152) of undoped counterpart, and even comparable to that (163) of the PZT-8 (temperature range of 20–232 °C). We further check the influence of the threshold (**Fig. S1**) and benchmark temperature (**Fig. S2**) on the temperature-stable range and S_d value. The results indicate that only slight difference arise when the benchmark temperature changed as 100 °C. In other cases, the prerequisites have no significant influence on the comparative results of S_d.

2.2 The enhanced and temperature-stable piezoelectricity in Sm-doped BF-BT ceramic

We next investigate the piezoelectricity and its temperature stability of Sm-doped BF-BT

View Article Online
DOI: 10.1039/D5TA09690A

ceramic. Here, optimal doping content was determined through a preliminary experiment, in which the $0.7BiFeO_3$-$0.3Ba_{1-x}Sm_xTiO_3$ (x from 0.00 to 0.04) ceramics were prepared and electrical properties were measured (**Fig. S3**). The result shows the $0.7BiFeO_3$-$0.3Ba_{0.99}Sm_{0.01}TiO_3$ has highest d_{33} value and dielectric permittivity at room temperature. **Fig. 3a** shows piezoelectric coefficients of undoped and Sm-doped BF-BT ceramics under various temperatures. On one hand, at room temperature, the d_{33} of the doped sample is about 175 pC/N, which is much higher than that of the undoped counterpart. On the other hand, the d_{33} of the undoped sample starts to fall once the temperature approaching 230 °C, as a comparison, the d_{33} of the doped one has no obvious decay until the temperature near 340 °C, indicates the better thermal stability. We further assess the reliability of piezoelectricity of the Sm-BF-BT ceramic. d_{33} of poled sample is measured three times during the heating process from 20 to 300 °C, as shown in **Fig. 3b**. In the measurement, the sample was cooled to 20 °C before the next test starts. We can see that d_{33} under second heating presents small difference compared to that under first measurement, and there is almost no difference between under third and second measurement, particularly in the temperature below 200 °C. These results suggested that Sm-doped BF-BT ceramic has a good thermal cycling stability.

View Article Online
DOI: 10.1039/D5TA09690A

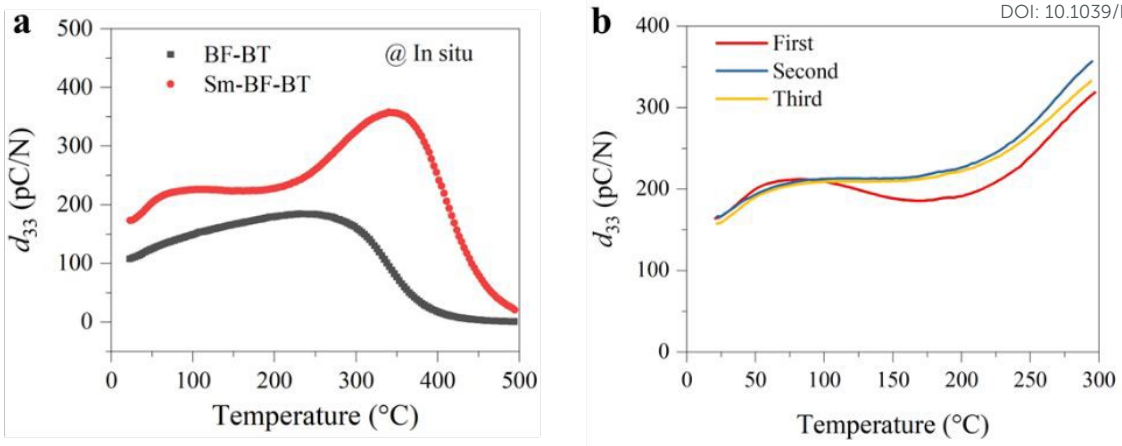

Fig. 3 Piezoelectricity of the lead-free BF-BT ceramics under various temperatures. **a**, The piezoelectric coefficient d_{33} of BF-BT and Sm doped BF-BT ceramics under 20–500 °C. **b**, The d_{33} of the Sm doped BF-BT ceramics under first, second and third heating cycles from 20 to 300 °C.

We not only improved the piezoelectricity at room temperature but also enhanced the temperature stability by doping. First, we explored the mechanism behind the improvement of piezoelectric properties. **Fig. 4a** shows the polarization-electric field (*P*-*E*) hysteresis loop of the poled samples. After doping, the *P*-*E* loop shrinks, accompanied by a decrease in coercive field and remnant polarization, but it still exhibits a high remnant polarization of 34 μC cm^{-2}. **Fig. 4b** shows their strain-electric field (*S*-*E*) loops, the asymmetric shape is because that the sample was pre-poled with a DC field before the measurement, causing the alignment of defect dipoles.[5, 21] It is noted that the direction of defect dipole is unchanged after the first electric treatment, but they can be stretched or contracted. The amplitude of strain is determined by the behaviors of defect dipole and spontaneous polarization.[5] The larger strain on the positive electric field is due to the initially applied electric field being same to the polarization direction of the sample. In this case, the defect dipole was stretched and spontaneous polarization was aligned along applied field. Under the negative electric field, the defect dipole was contracted

View Article Online
DOI: 10.1039/D5TA09690A

and spontaneous polarization was also aligned along applied field. Despite that, *P*-*E* loop is almost symmetric because that the effect of defect dipole and spontaneous polarization on measured polarization is same regardless of the direction of applied electric field.[5] From **Fig. 4b**, we can also observe a decrease in coercive field and a significant increase in strain for the doped sample. We further measured the strain under unipolar electric field. As shown in **Fig. 4c**, the doped sample exhibited a larger unipolar strain, corresponding to an increase in the piezoelectric strain coefficient from 206 to 249 pm V^{-1}. The macroscopic electrical properties are closely related to the microstructure and domain structure of the crystals.[2, 31] We observed the domain structure of the samples using piezoresponse force microscopy, as shown in **Figs. 4d** and **4e**. Both samples exhibited clear ferroelectric domain morphology, the regular lamellar/strip domains dominate.[32] Interestingly, the domain size significantly decreased, and the domain density increased after doping. This may be related to the reduced grain size (**Fig. 4e** and **Fig. S4**) and altered crystal structure.[33, 34]

View Article Online
DOI: 10.1039/D5TA09690A

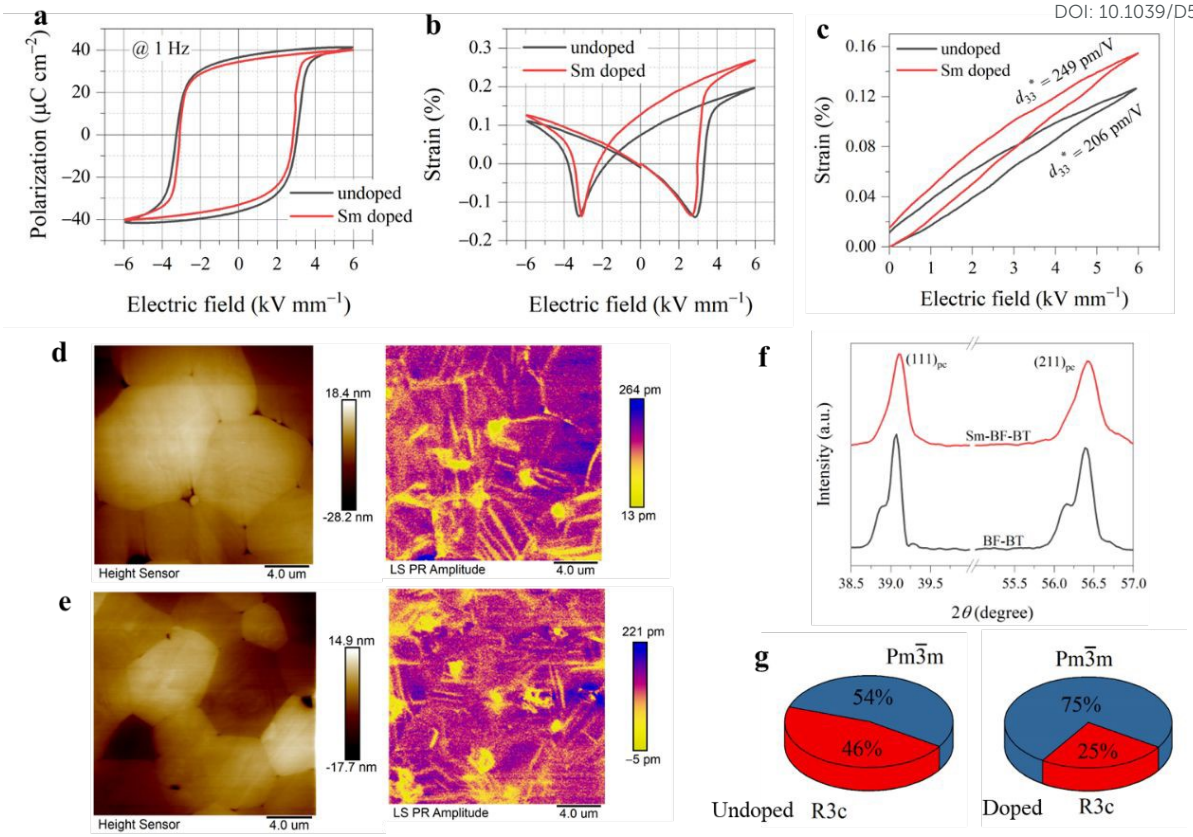

Fig. 4 The electrical properties and microstructure at room temperature. The polarization (**a**) and strain (**b**) of undoped and Sm-doped samples under the bipolar electric field at 1 Hz. **c**, The unipolar strain at 1 Hz. The surface topography and piezoelectric amplitude images of the undoped (**d**) and Sm-doped (**e**) samples observed by a piezoresponse force microscope. **f**, The X-ray diffraction patterns. **g**, The phase content obtained by the Rietveld refinement.

Fig. 4f and **Fig. S5** show the X-ray diffraction patterns of the samples, both undoped and doped samples exhibit pure perovskite phase. After doping, the diffraction peaks shift towards higher angles, indicating a decrease in lattice volume. This is due to that Sm^{3+} (1.24 Å) has a smaller radius compared to Ba^{2+} (1.61 Å).[35] Additionally, it can be observed that the split diffraction peaks become less pronounced after doping. It has been reported that 0.7BF-0.3BT exhibits a crystal structure with coexisting rhombohedral *R*3*c* and pseudo-cubic $Pm\bar{3}m$

View Article Online
DOI: 10.1039/D5TA09690A

phases.[36, 37] We performed fitting of the patterns using a mixed-phase of *R*3*c* and $Pm\bar{3}m$. It can be observed that the content of the *R*3*c* phase significantly decreases after doping (**Fig. 4g and Table S1**), indicating an enhanced symmetry of the crystal structure. Previous reports have indicated that differences in valence and ionic radii lead to discontinuities in crystal structure and polarization,[2] increasing the interfacial energy of the system. Competition between the bulk and interfacial energy may lead to a flattened free-energy profile,[38] consistent with the enhanced symmetry of the crystal structure and reduced domain size. In addition, the higher electronegativity of Sm^{3+} compared to Ba^{2+} increases the degree of local covalent bonding, and the hybridization of ionic and covalent bonds can also promote the piezoelectricity.[11]

Second, we investigate the origin of enhanced thermal stability. It is well known that the Curie temperature of a ferroelectric is a critical factor affecting the stability of the piezoelectricity.[30] **Fig. 5a** and **Fig. S6** present the temperature-dependent dielectric permittivity and loss of undoped and doped BF-BT ceramics. We can see that the undoped sample presents a high Curie temperature of ~510 °C. After doping, the Curie temperature decreases to ~490 °C. Generally, a higher Curie temperature corresponds to a higher thermal depolarization temperature and thus greater stability of the piezoelectric performance.[30] However, in our work, the doped sample exhibits the higher operating temperature and enhanced piezoelectric stability (**Fig. 3a**). First, the temperature stability of electrical properties depends on the lattice symmetry, a ferroelectric with low lattice symmetry presents a large fluctuation with the temperature due to the fragmentation of long-range ferroelectric order. For ferroelectric with high symmetry, the change is usually smooth.[39] In the BFO-based systems, there were multiple phase transitions

View Article Online
DOI: 10.1039/D5TA09690A

from room temperature to the Curie temperature.[40] After doping, the lattice symmetry increased, phase transition becomes less abrupt, thus the stabilities of dielectric permittivity and piezoelectricity were highly improved. As shown in **Fig. S6**, we can find that a small hump near 300 °C disappeared after Sm doping. Second, the point defect, such as oxygen vacancy is also vital factor that affects the temperature stability. By comparing the dielectric permittivity and loss at a lower temperature range (**Figs. 5b-c**), we can see that the undoped sample exhibits extremely unstable dielectric properties, particularly in terms of dielectric loss, where an obvious rise occurs at temperatures near 100 °C. Dielectric loss originates from electrically active regions such as point defects.[41] For BF-based materials, the bismuth volatilization, reduction of iron ions, and self-decomposition of BF can lead to the generation of oxygen vacancies.[42] In contrast, the doped sample shows significantly enhanced stability in dielectric properties, with a dielectric loss below 0.1 in the temperature range from room temperature to 250 °C.

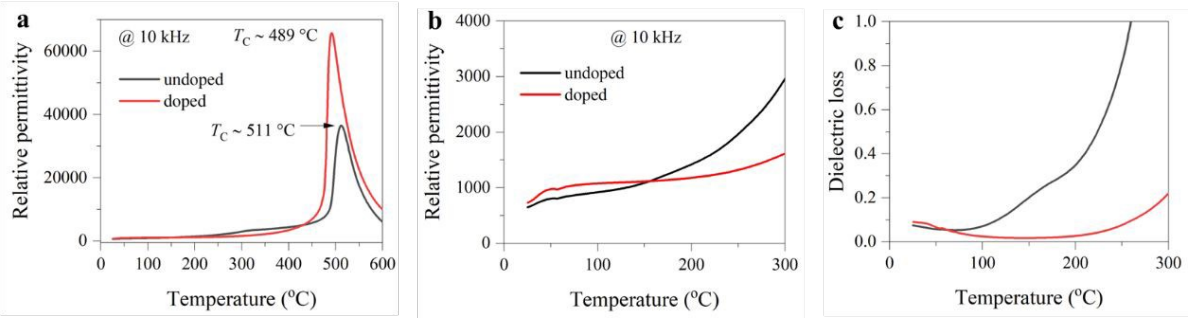

Fig. 5 The dielectric properties of BF-BT samples. a, The temperature-dependent dielectric permittivity at 10 kHz. **b-c,** The dielectric permittivity (**b**) and loss (**c**) from 20 °C to 300 °C, showing more stable dielectric properties after the Sm doping.

To further identify the point defects, we measured the impedance spectra of the samples at elevated temperatures. **Fig. 6a** displays the impedance complex plane plots of the undoped

View Article Online
DOI: 10.1039/D5TA09690A

sample. Interestingly, we observe two semicircular arcs, indicating that the impedance of the sample is composed of two different electrical responses,[43] namely grain and grain boundary in the order of decreasing frequency. In contrast, in the doped sample, only a single arc can be observed in this temperature range, as shown in **Fig. 6b.** An electrical response implies that the resistance of grains in doped sample is much larger than that in undoped sample, thereby the resistance of grains and grain boundaries are comparable. Previous reports pointed out the presence of a core-shell microstructure in BF-BT-based ceramics,[44] consisting of an electrically active core and a resistive shell. As shown in **Fig. S7**, we can observe dark shells and bright cores within individual grains, representing Ba, Ti rich and Bi, Fe rich regions, respectively. The electrically active cores may be attributed to an abundance of defects.[44] Additionally, we find that the resistance (the intersection points of the arc and the X-axis) of the doped sample increases by an order of magnitude than the undoped counterpart at the same temperature. To further understand the defect dynamics, quantitative analysis was conducted. The measured impedance spectra were fitted according to an equivalent circuit, for undoped sample, the circuit consisting of two parallel resistance (R) and constant phase (Q) elements connected in series (**Fig. S8**) was adopted,[45] while only a parallel R and Q element was required in doped sample due to single arc. The fitted curves are displayed in **Fig. S9**. Based on previous report,[45] the temperature dependence of the conductivities of undoped and doped ceramics were calculated and presented in **Fig. 6c** and **d**. The conductivities of two specimens roughly show an Arrhenius-type behavior.[46, 47] It can be observed that the conductivity of the Sm doped sample is significantly lower than those of the undoped sample (core and shell). Moreover,

View Article Online
DOI: 10.1039/D5TA09690A

corresponding activation energies (E_a) derived from Arrhenius equation[46] are given and shown in the **Fig. 6c** and **d**. For the undoped sample, core and shell activation energies is 0.69 eV and 0.89 eV, respectively. As a comparison, activation energy (1.08 eV) for Sm doped sample is much higher than those of the undoped one. The increased *E*a further proves a decrease in oxygen vacancy concentration.[48]

In the BF-based system, both the reduction of Fe^{3+} and volatilization of Bi^{3+} lead to a decrease in positive charge.[42] To maintain the electrical neutrality, extra oxygen vacancies are generated, defect chemistry can be represented as:

$$2BiFeO_3 \rightarrow 2Fe_{Fe}^{\times} + 3O_O^{\times} + 2V_{Bi}^{'''} + 3V_O^{\bullet\bullet} + Bi_2O_3 \uparrow$$

$$4BiFeO_3 \rightarrow 4Bi_{Bi}^{\times} + 10O_O^{\times} + 4Fe_{Fe^{3+}}^{2+\prime} + 2V_O^{\bullet\bullet} + O_2 \uparrow$$

These oxygen and cation vacancies are coupled to form defect dipoles, which increase the conductivity of the ceramic and form leakage currents, especially in high temperatures or strong electric fields. With the introduction of Sm^{3+} ions in Ba-site, compensating positive charges mitigate the generation of oxygen vacancies as the formula:[42]

$$2Sm_2O_3 \xrightarrow{Ba^{2+}} 4Sm_{Ba}^{\bullet} + 8O_O^{\times} - 2V_O^{\bullet\bullet} - O_2 \uparrow$$

Where the symbol "–" represents the decrease, extra positive charges due to the Sm^{3+} substitution in the Ba-site lead to decreased concentration of oxygen vacancies. To provide direct experimental evidence, the X-ray photoelectron spectroscopy (XPS) test was conducted on the undoped and doped ceramic powders, as shown in **Fig. S10**. The splitting of the O1s signals observed in the XPS spectra indicates that the oxygen vacancy. It was found that the shoulder peak became less obvious after Sm-doping. Furthermore, the quantification analysis

View Article Online
DOI: 10.1039/D5TA09690A

of the element show that the relative content of oxygen in doped sample (52%) is higher than that in undoped one (48%), implying the decrease of oxygen vacancy concentration.

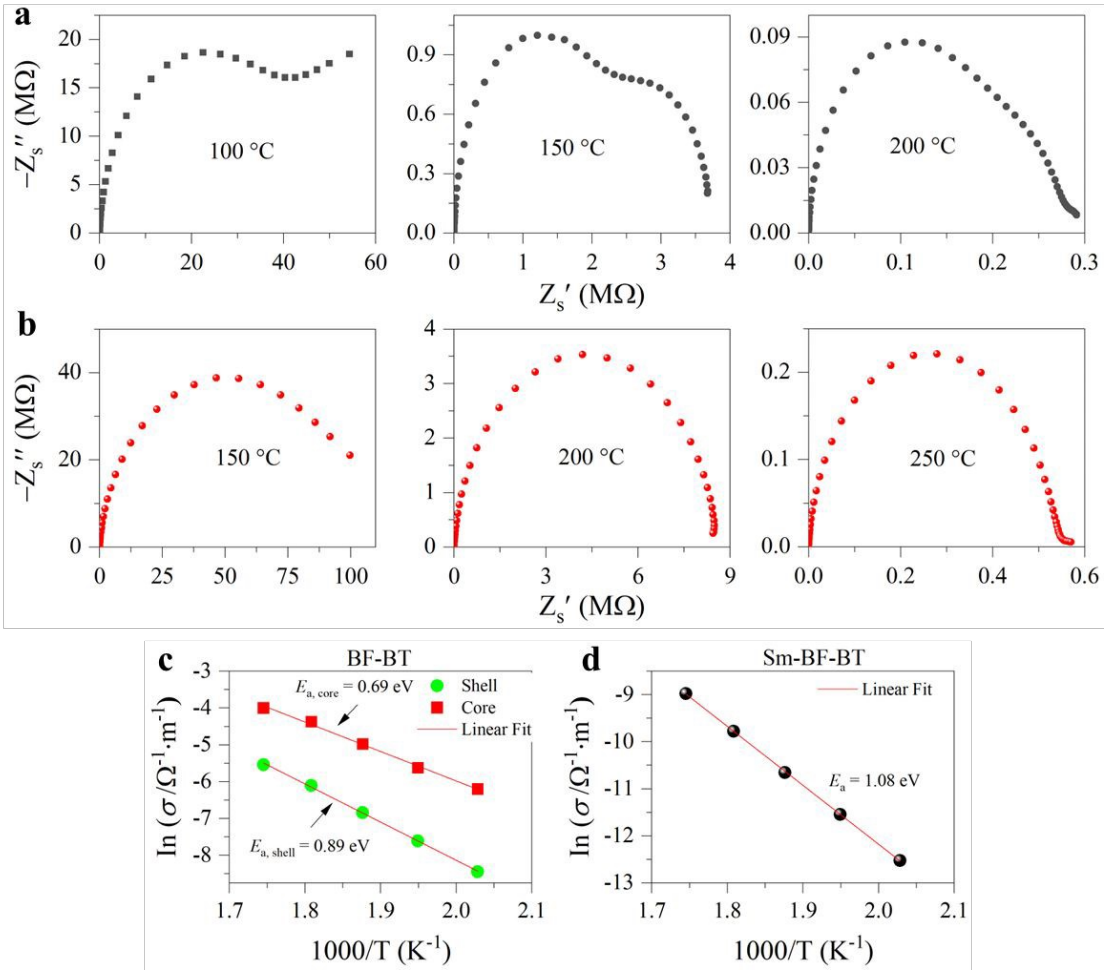

Fig. 6 The high-temperature impedance and defect chemistry analysis. Impedance complex plane plots for the undoped (**a**) and doped (**b**) samples at various temperatures. **c**, Core and shell conductivities of the BF-BT ceramic. **d**, Bulk conductivity of the Sm-doped BF-BT ceramic. The solid line is a result of linear least-square fitting.

After Sm doping, the main defect dipoles $V_{Bi}''' - V_O^{\bullet\bullet}$ and $Fe_{Fe^{3+}}^{2+\prime} - V_O^{\bullet\bullet}$ in perovskite ABO_3 structure were changed to $V_{Bi}''' - Sm_{Ba}^{\bullet}$ and $Fe_{Fe^{3+}}^{2+\prime} - Sm_{Ba}^{\bullet}$. Among them, $V_{Bi}''' - V_O^{\bullet\bullet}$ and $Fe_{Fe^{3+}}^{2+\prime} - V_O^{\bullet\bullet}$ are along <110> and <001> directions,[49] the defect dipole reorientation needs only 1 step of $V_O^{\bullet\bullet}$migrations.[5] As a comparison, both $V_{Bi}''' - Sm_{Ba}^{\bullet}$ and $Fe_{Fe^{3+}}^{2+\prime} - Sm_{Ba}^{\bullet}$ are along

View Article Online
DOI: 10.1039/D5TA09690A

<111> directions, which is consistent with the directions of ferroelectric polarization in rhombohedral phase.[3] $Fe'_{Fe^{3+}}-Sm^{g}_{Ba}$ cannot move due to absence of ion exchange channels, the V'''_{Bi} in defect dipole $V'''_{Bi}-Sm^{g}_{Ba}$ needs 2 steps of migrations to realize reorientation, and cost much more energy. Therefore, it is more difficult for Sm-doped BF-BT to depolarize, which will contribute to improved thermal stability at high temperature.

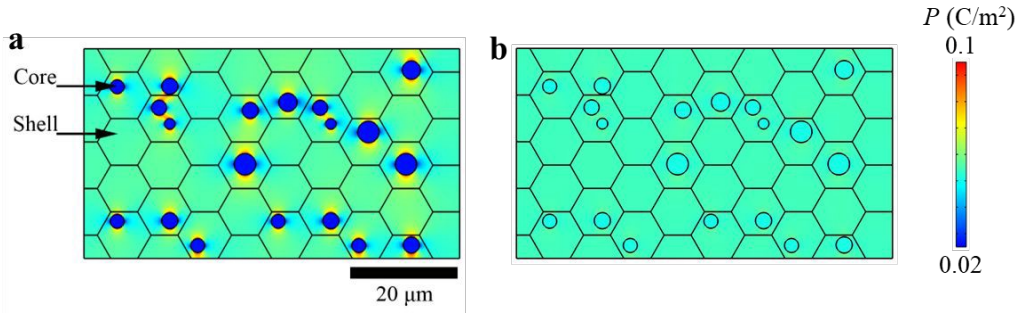

Fig. 7 The polarization distribution for the electrically heterogeneous (a) and homogeneous (b) dielectrics simulated by the COMSOL Multiphysics. For the former, the conductivity of the core is much higher than the shell. For the latter, the conductivity of both is almost the same.

To investigate the impact of electrical homogeneity on the poling process and piezoelectric properties, we developed two physical models (**Fig. S11** and **Table S2**). The first model consists of a conducting core and an insulating shell, simulating the undoped sample, while the second model features a core with conductivity similar to that of the shell, representing the doped sample. Using COMSOL 6.1 (Physics of current), we analyzed the polarization distribution (**Fig. 7**). Our results show that in electrically inhomogeneous dielectrics, the conducting core exhibits minimal polarization (**Fig. 7a**), as the electric field is primarily concentrated in regions with higher resistivity (**Fig. S11**). In contrast, electrically homogeneous dielectrics display more uniform polarization distribution in entire regions (**Fig. 7b**). Furthermore, the high-temperature

View Article Online
DOI: 10.1039/D5TA09690A

ferroelectric measurements support these findings. As shown in **Fig. S12**, the undoped sample begins to exhibit leakage at 50 °C, whereas the doped sample remains stable until 150 °C. The significant leakage in the undoped sample leads to insufficient alignment of ferroelectric domains, which is reflected in the impedance and phase spectrum at the resonance frequency (**Fig. S13**).[50] Notably, the maximum phase angle of the doped sample is significantly higher than that of the undoped sample. Our results clearly demonstrate that stable piezoelectricity at high temperatures is attributed to enhanced electrical homogeneity and reduced conductivity.

3. Conclusion

We introduce a novel metric to quantitatively assess the temperature stability of piezoelectricity, where exceptional temperature stability is characterized by a broad temperature range and high operating temperature concurrently. This metric has been validated for both commercial PZTs and lead-free piezoelectric materials. Although the temperature stability of lead-free Sm-doped BF-BT ceramics is inferior to that of commercial PZT-4 and PZT-5A, it surpasses that of commercial PZT-8. Notably, the enhanced temperature stability in Sm-doped BF-BT ceramic, compared to its undoped counterpart, is attributed to the suppression of electrical inhomogeneity resulting from a reduction in defect concentration. This work is poised to serve as a paradigm for the design of high-temperature piezoelectrics and pave the way for the development of high-temperature electronic devices.

4. Materials and methods

4.1 Material preparation

The $0.7BiFeO_3$-$0.3Ba_{1-x}Sm_xTiO_3$ (x = 0, 0.01, 0.02, 0.03, 0.04) ceramics were prepared by

View Article Online
DOI: 10.1039/D5TA09690A

conventional solid-state reaction. The raw powders, Bi_2O_3, Fe_2O_3, $BaCO_3$, TiO_2 and Sm_2O_3 are dried and then weighed according to the stoichiometric ratio. The powders are mixed by ball milling in ethanol. The dried mixture was calcined at 800 °C for 6 h, and then was refined by ball milling in ethanol. The 5% PVA solution was added into the dried powder. The powders were formed into pellets by uniaxial pressing of ~200 MPa, followed by binder burn-out at 600 °C. The samples were sintered at 980–1020 °C for 3 h. All sintered ceramics were annealed at 800 °C for 2 h in the air atmosphere and was followed by an air-quenching process before the temperature drops. Subsequently, the surfaces of samples were ground. Silver electrodes were prepared by magnetron sputter (Q150T ES Plus, Quorum Technologies), followed by annealing at 400 °C. The samples were poled under the electric field of 4.5–5 kV mm^{-1} at 80–120 °C for 30 min. After aged for 24 h, the electrical properties were measured.

The commercial PZTs (PZT-5A, PZT-4 and PZT-8) are purchased from the Zhuhai Jiaming Electronic Technology Co., Ltd..

4.2 Material characterizations

The bulk densities of the ceramics were measured by a density meter (XS104, Mettler Toledo, Switzerland). The crystal structures of the powder samples were examined with X-ray diffraction (D8 advance, Bruker). The lattice parameters and phase content were analyzed with a Rietveld refinement software (Topas 3.0). The morphology and grain size of the sample were observed by a scanning electron microscope (Quanta 450, FEI). To observe the ferroelectric domain, the electrodes of the poled sample were ground off and the surfaces were polished. The ferroelectric domains were identified with an atomic force microscope (Dimension Icon with

View Article Online
DOI: 10.1039/D5TA09690A

ScanAsyst, Bruker) in an optimized vertical domains mode. In the measurement, a conductive probe (Asyelec.02-R2, Asylum research) is utilized. Chemical states of oxygen were detected by X-ray photoelectron spectroscopy (Axis Supra+, Kratos Analytical).

The capacitance and loss of poled sample were tested with an inductance capacitance resistance meter (E4980A, Agilent Technologies) at temperatures of 20–600 °C with a heating rate of 3°C min^{-1}. The ferroelectric polarization and electric-field induced strain were measured by a ferroelectric test system (CPE1801, PolyK Technologies) equipped with a fotonic sensor (MTI2100, MTI Instruments). The high-temperature impedance in the frequency range of 10^{-2} Hz to 10^{7} Hz was measured by a broadband impedance spectrometer (Concept 40, Novocontrol Technologies) under a small alternating voltage of 1 V_{RMS}, the impedance spectra were fitted by a commercial software (ZSimpWin). The piezoelectric charge coefficients at various temperature were test with an in-situ quasi-static d_{33} meter (TZFD-600, Harbin Julang Technology), the heating rate is 3 °C min^{-1}. The impedances and phase angles of poled samples near the resonance frequency were observed by an ENA network analyzer (E5061B, Keysight).

References

1. G. H. Haertling, J. Am. Ceram. Soc., 1999, 82, 797-818.
2. F. Li, D. B. Lin, Z. B. Chen, Z. X. Cheng, J. L. Wang, C. C. Li, Z. Xu, Q. W. Huang, X. Z. Liao, L. Q. Chen, T. R. Shrout and S. J. Zhang, Nature materials, 2018, 17, 349-354.
3. X. Ren, Nature materials, 2004, 3, 91-94.
4. Y. Dong, K. Zou, R. Liang and Z. Zhou, Prog. Mater. Sci., 2023, 132, 101026.
5. G. Huangfu, K. Zeng, B. Wang, J. Wang, Z. Fu, F. Xu, S. Zhang, H. Luo, D. Viehland and Y. Guo, Science, 2022, 378, 1125-1130.
6. J. Rödel, K. G. Webber, R. Dittmer, W. Jo, M. Kimura and D. Damjanovic, J. Eur. Ceram. Soc., 2015, 35, 1659-1681.
7. J. Wu, D. Xiao and J. Zhu, Chem. Rev., 2015, 115, 2559-2595.
8. S. Kim, R. Miyauchi, Y. Sato, H. Nam, I. Fujii, S. Ueno, Y. Kuroiwa and S. Wada, Adv. Mater., 2023, 35, 2208717.

9. M.-H. Zhang, C. Shen, C. Zhao, M. Dai, F.-Z. Yao, B. Wu, J. Ma, H. Nan, D. Wang, Q. Yuan, L. L. da Silva, L. Fulanović, A. Schökel, P. Liu, H. Zhang, J.-F. Li, N. Zhang, K. Wang, J. Rödel and M. Hinterstein, Nat. Commun., 2022, 13, 3434.
10. G. Wang, T. Hu, W. Zhu, Z. Lu, A. Kleppe, M. Diaz Lopez, A. Feteira, D. C. Sinclair, Z. Fu, H. Huang, D. Wang and I. M. Reaney, Phys. Rev. Lett., 2023, 130, 076801.
11. Y. Saito, H. Takao, T. Tani, T. Nonoyama, K. Takatori, T. Homma, T. Nagaya and M. Nakamura, Nature, 2004, 432, 84-87.
12. M. Waqar, H. Wu, J. S. Chen, K. Yao and J. Wang, Adv. Mater., 2022, 34, 2106845.
13. J. Wu, Z. Fan, D. Xiao, J. Zhu and J. Wang, Prog. Mater. Sci., 2016, 84, 335-402.
14. J. Wu, J. Appl. Phys., 2020, 127, 190901.
15. D. Wang, G. Wang, S. Murakami, Z. Fan, A. Feteira, D. Zhou, S. Sun, Q. Zhao and I. M. Reaney, J. Adv. Dielectr., 2018, 08, 1830004.
16. Z. Shen, J. Guo, X. Gao, W. Xuan, J. Zhang, D. Wang, J. Cheng, S. Zhang and J. Chen, Journal of Materiomics, 2025, 11, 100946.
17. H. Li, J. Zhao, Y. Li, L. Chen, X. Chen, H. Qin, H. Zhou, P. Li, J. Guo and D. Wang, ACS Applied Materials & Interfaces, 2024, 16, 9078-9087.
18. M. H. Lee, D. J. Kim, J. S. Park, S. W. Kim, T. K. Song, M.-H. Kim, W.-J. Kim, D. Do and I.-K. Jeong, Adv. Mater., 2015, 27, 6976-6982.
19. J. Chen, J. E. Daniels, J. Jian, Z. Cheng, J. Cheng, J. Wang, Q. Gu and S. Zhang, Acta Mater., 2020, 197, 1-9.
20. G. Wang, Z. Fan, S. Murakami, Z. Lu, D. A. Hall, D. C. Sinclair, A. Feteira, X. Tan, J. L. Jones, A. K. Kleppe, D. Wang and I. M. Reaney, J. Mater. Chem. A, 2019, 7, 21254-21263.
21. J. Lin, F. Lv, Z. Hong, B. Liu, Y. Wu and Y. Huang, Adv. Funct. Mater., 2024, 34, 2313879.
22. W. Jia, Y. Hou, M. Zheng, Y. Xu, M. Zhu, K. Yang, H. Cheng, S. Sun and J. Xing, IET Nanodielectr., 2018, 1, 3-16.
23. W. Jia, Y. Hou, M. Zheng, Y. Xu, X. Yu, M. Zhu, K. Yang, H. Cheng, S. Sun and J. Xing, J. Am. Ceram. Soc., 2018, 101, 3468-3479.
24. *Ceramic dielectric capacitors classes I, II, III, and IV. Part 1, Characteristics and requirements*, Electronic Components, Assemblies & Materials Association, EIA, Arlington, VA, 2002.
25. J.-S. Zhou, K. Wang, F.-Z. Yao, T. Zheng, J. Wu, D. Xiao, J. Zhu and J.-F. Li, Journal of Materials Chemistry C, 2015, 3, 8780-8787.
26. T. Zheng, H. J. Wu, Y. Yuan, X. Lv, Q. Li, T. L. Men, C. Zhao, D. Q. Xiao, J. G. Wu, K. Wang, J. F. Li, Y. L. Gu, J. Zhu and S. J. Pennycook, Energy Environ. Sci., 2017, 10, 528-537.
27. X. D. Yan, M. P. Zheng, X. Gao, M. K. Zhu and Y. D. Hou, Acta Mater., 2020, 187, 29-40.
28. W. F. Liu and X. B. Ren, Phys. Rev. Lett., 2009, 103, 257602.
29. D. Xue, Y. Zhou, H. Bao, C. Zhou, J. Gao and X. Ren, J. Appl. Phys., 2011, 109, 054110.
30. M. Fang, S. Rajput, Z. Dai, Y. Ji, Y. Hao and X. Ren, Acta Mater., 2019, 169, 155-161.
31. C. R. Qiu, B. Wang, N. Zhang, S. J. Zhang, J. F. Liu, D. Walker, Y. Wang, H. Tian, T.

View Article Online
DOI: 10.1039/D5TA09690A

R. Shrout, Z. Xu, L. Q. Chen and F. Li, Nature, 2020, 577, 350-354.
32. B. Xun, A. Song, J. Yu, Y. Yin, J. F. Li and B. P. Zhang, ACS applied materials & interfaces, 2021, 13, 4192-4202.
33. P. Zheng, J. L. Zhang, Y. Q. Tan and C. L. Wang, Acta Materialia, 2012, 60, 5022-5030.
34. D. Ghosh, A. Sakata, J. Carter, P. A. Thomas, H. Han, J. C. Nino and J. L. Jones, Adv. Funct. Mater., 2014, 24, 885-896.
35. R. D. Shannon, Acta Crystallographica, 1976, 32, 751-767.
36. M. M. Kumar, A. Srinivas and S. V. Suryanarayana, Journal of Applied Physics, 2000, 87, 855-862.
37. S. Kim, G. P. Khanal, H.-W. Nam, I. Fujii, S. Ueno, C. Moriyoshi, Y. Kuroiwa and S. Wada, Journal of Applied Physics, 2017, 122, 164105.
38. Y. Nahas, A. Akbarzadeh, S. Prokhorenko, S. Prosandeev, R. Walter, I. Kornev, J. Iniguez and L. Bellaiche, Nature communications, 2017, 8, 15944.
39. F.-Z. Yao, K. Wang, W. Jo, K. G. Webber, T. P. Comyn, J.-X. Ding, B. Xu, L.-Q. Cheng, M.-P. Zheng, Y.-D. Hou and J.-F. Li, Adv. Funct. Mater., 2016, 26, 1217-1224.
40. D. V. Karpinsky, M. V. Silibin, S. V. Trukhanov, A. V. Trukhanov, A. L. Zhaludkevich, S. I. Latushka, D. V. Zhaludkevich, V. A. Khomchenko, D. O. Alikin, A. S. Abramov, T. Maniecki, W. Maniukiewicz, M. Wolff, V. Heitmann and A. L. Kholkin, Nanomaterials, 2020, 10, 801.
41. G. Liu, S. Zhang, W. Jiang and W. Cao, Mater. Sci. Eng. R, 2015, 89, 1-48.
42. M. Habib, P. Ahmad, F. Akram, I. Kebaili, A. Rahman, I. U. Din, M. Javid Iqbal, M.-H. Kim, S. Lee, M. Uddin Khandaker, H. Goo Yeo, A. Karoui and T. K. Song, Ceram. Int., 2022, 48, 26608-26617.
43. N. Hirose and A. R. West, J. Am. Ceram. Soc., 1996, 79, 1633-1641.
44. G. Wang, J. Li, X. Zhang, Z. Fan, F. Yang, A. Feteira, D. Zhou, D. C. Sinclair, T. Ma, X. Tan, D. Wang and I. M. Reaney, Energy Environ. Sci., 2019, 12, 582-588.
45. X. Guo and Z. Zhang, Acta Materialia, 2003, 51, 2539-2547.
46. F. D. Morrison, D. C. Sinclair and A. R. West, J. Am. Ceram. Soc., 2001, 84, 531-538.
47. Y. Deng, J. Dai, Z. Fan, W. Yue, F. Huang, A. A. Mohamad, A. Evcin, Y. Tabak, G. Abdurakhmanov, M. Abu Abdeen and D. Wang, Ceramics International, 2025, 51, 55067-55072.
48. O. Raymond, R. Font, N. Suarez-Almodovar, J. Portelles and J. M. Siqueiros, J. Appl. Phys., 2005, 97, 084107.
49. Z. Zhao, Y. Lv, Y. Dai and S. Zhang, Acta Materialia, 2020, 200, 35-41.
50. B.-W. Xun, N. Wang, B.-P. Zhang, X.-Y. Chen, Y.-Q. Zheng, W.-S. Jin, R. Mao and K. Liang, Ceram. Int., 2019, 45, 24382-24391.

Conflicts of interest

There are no conflicts to declare.

View Article Online
DOI: 10.1039/D5TA09690A

Data availability

All the data have been presented in the manuscript and supplementary information.

Acknowledgments

The research was supported by the National Natural Science Foundation of China (Project No. T2522031), the Hong Kong Research Grants Council (General Research Fund Project No. 16214025), and the Innovation and Technology Fund (Project No. ITS/232/24) of the Innovation and Technology Commission, the Government of the Hong Kong Special Administrative Region. We thank Prof. Dragan Damjanovic for revising the manuscript.

View Article Online
DOI: 10.1039/D5TA09690A

Data availability Statement

All the data have been presented in the manuscript and supplementary information.